Thermophysics and Aeromechanics, *2024*, *Vol. 31*, *No. 2*

DOI: 10.1134/S0869864324020069

Steady and unsteady numerical investigation of mixed convective heat transfer enhancement in a channel with baffles attached to the heated wall

H. Toumi, R. Henniche, and A. Korichi

University of Medea, *Medea*, *Algeria*

E-mail: rabahh200@yahoo.fr

(*Received July 30*, *2021*; *revised October 11*, *2021*;
accepted for publication December 9, *2021*)

Numerical computation of aiding mixed convection and heat transfer characteristics in a channel with a baffled heated wall is carried out in this work. The equations of mass, momentum and energy, alongside the boundary conditions, are solved by the finite volume formulation using the open source OpenFOAM® code. Simulations are accomplished under different parameter combinations, including the Reynolds number, Grashof number, and baffle dimension. The results are presented in terms of streamlines, isotherm contours, Nusselt number, and friction factor. The results obtained revealed that the flow translates from steady to unsteady state at a relatively low value of Reynolds number. The unsteady flow behaviour contributes to improve heat transfer by disturbing the near-wall region. The augmentation of velocity and baffle dimension leads to a notable heat transfer enhancement; however, this enhancement is less sensitive to the heating intensity augmentation.

Keywords: mixed convection, unsteady flow, baffles, numerical simulation, OpenFOAM.

Introduction

The heat transfer process is encountered in different natural and industrial applications where the process involves the energy transfer via the heat conduction, like compact heat exchangers, solar collectors systems, chemical reactors, electronic cooling. Thermal management includes reducing heat losses or enhancing heat exchange in such systems and has been the subject of interest for many scientists for several decades. From previous works, several methods can be employed to achieve heat transfer enhancement: passive methods by the perturbation of the near-wall region using vortex generators (bar, cylinder, fins …) and active methods using moving objects or modulated flows cited by [1–4].

Patankar et al. [5] to the best of the authors' knowledge were the first to interest in the numerical investigation of heat convection and fluid flow in finned channel. Later, many works have dealt with the utility of fins in devices that involve the transfer of energy in the form of heat. Webb and Ramadhyani [6] studied the heat convection in a two parallel plates channel with baffles in offset configuration under laminar flow regime. They found that, after

© H. Toumi, R. Henniche, and A. Korichi, 2024

a finite length from the inlet, the flow became periodically fully developed. They also found that a considerable increase in Nusselt number is obtained for a fluid of high Prandtl numbers, such as water. Besides, the conduction in channel walls plays a significant role in increasing heat transfer. Berner et al. [7] conducted an experimental research inspection of the air flow in a channel with ten transverse baffles fixed alternately on the two walls. Laminar flow behaviour has been noticed with a Reynolds number lower than 600.

Cheng et al. [8] analysed the buoyant flow effect on the heat exchange and fluid dynamics pattern in a channel including a series of identical conductive equi-spaced fins heated asymmetrically. The heat boundary condition is imposed to finned wall where there is a periodic flow feature reign in the fully developed region. Their results showed that vortex intensity and configuration are governed by the Grashof number, Reynolds number, and geometric parameters including the space between the baffles, their heights, and the channel tilt angle. Cheng and Yang [9] studied the heat convection and fluid flow characteristics taking into account the free convection contribution in a developing vertical parallel-plates flow channel with fin array. Their results proved the periodic variation of the flow after certain modules from the inlet. They noticed that, if the wall's heating is strong enough, an opposite pressure gradient can be developed in the downstream channel, and a series of vortices can appear next to the cold wall.

Fung and Lazaridis [10] found that in addition to the flow recirculation downstream of each baffle, the buoyant flow effect generates a vortex in the vicinity of the cold wall with the tendency to tone down heat transfer. The main vortex behind the fin of the hot wall expands with the Reynolds number, while the secondary vortex located near the cold wall is suppressed. This phenomenon reduces heat transfer at the hot wall and distorts the temperature profile development, the heat transfer degradation became even more pronounced as the Prandtl number raises. The geometric parameters affect both heat transfer and friction at the two walls of the channel.

The effect of a baffle on mixed convection under opposing effect in a vertical channel under pulsating flow has been examined by Chang and Shiau [11]. The effect of pulsation frequency, Prandtl number, and baffle position is explored for different Richardson number (Ri) values. The results accentuate that heat transfer is better when using a partition and pulsating flow. The global Nusselt number enlarges for large values of Reynolds number, pulsation amplitude, and Prandtl number. Cheng and Huang [12] studied the pure forced convection between two parallel plates with transverse fins (baffles) asymmetrically placed. Their results emerged that the relative position of the baffle rows is a factor influencing the flow field, particularly for large size baffles. Tsay et al. [13] examined the heat transfer enrichment due to the insertion of a transverse baffle in a channel with backward-facing step. The effect of baffle size, thickness, and spacing of the baffle regarding to backward-facing step on the flow characteristics is investigated for Reynolds number values in the range of 100 to 500. Their findings proved that the placement of a baffle in the channel can increase the global Nusselt number up to 190%. Moreover, they illustrated that the heat transfer rate and fluid flow patterns are greatly dependent on the baffle position.

Mousavi and Hooman [14] affirmed that the increase of Reynolds and Prandtl numbers increases the Nusselt number along the isothermal channel walls in a horizontal position with alternated baffles. Santos and Lemos [15] presented a numerical study on laminar flow in a channel equipped with solid or porous baffles. They stood out that solid baffles led to a more considerable improvement than porous baffles. However, they augment the friction factor.

The use of porous and solid baffles attached to both walls in an offset manner investigated by Zhang et al. [16]. Their results asserted that the baffles cause a flow separation/

/attachment, which affects the local heat transfer efficiency. They also found that the rate of evacuated heat when using the solid baffles is much more significant compared to that for porous baffles. Ko et al. [17] conducted a numerical study on the utility of porous baffles, which induces an increase in heat exchange coefficient of up to 300%. Lopez et al. [18, 19] studied the dynamic and thermal effects numerically as a function of the location of normal baffles within a 3D channel. Their findings showed that the three-dimensional effect on the friction factor became more pronounced at large Reynolds number values.

Guo and Anand [20] studied three-dimensional convective heat transfer flow in a channel with one baffle near the inlet region. As general findings, the separation length upstream of the baffle and recirculating zone length downstream of the baffle increased with increasing in the Reynolds number and the dimension of the baffle. Recently, Tehrani and Abadi [21] presented a study on the dynamic and thermal behaviour of flow in a duct equipped with a series of baffles. Their results showed that baffle-type obstacles are rather ineffective for large values of the blocking ratio. Some experimental investigations were achieved to study the effect of baffles/fins on heat transfer and fluid flow, but their number is limited compared to the numerical ones. These investigations are limited to the global characteristics as the mean Nusselt number or the channel's friction factor, due to the experimental difficulties. An experimental work for turbulent flow with heat transfer in a rectangular baffled channel has been performed by Molki et al. [22]. They found that the augmentation of baffle dimension increases more the pressure losses and also increases the heat exchange coefficient. Fluid flow characteristics and thermal transfer with the periodic staggered baffles in a rectangular duct have been experimentally investigated by Habib et al. [23]. Uniform heat flux boundary condition is applied to both lower and upper walls. The experimental findings indicated that pressure loss increases with baffle size. For a given flow rate, the global and local heat transfer coefficients increase with augmenting Reynolds number. Habib et al. [23] also found that the heat exchange coefficient and the friction coefficient increase with increasing distance between baffles.

Yuan et al. [24] studied the heat transfer and dynamics of the flow experimentally in a duct with periodic rectangular fins along the main flow direction. They concluded an augmentation in heat transfer compared to the results obtained for a smooth duct. Recently, Terekhov et al. [25] showed that the installation of ribs on the channel walls reduces considerably the heat transfer and the buoyancy induced flow under natural convection regime, particularly at low Rayleigh number. Henniche and Korichi [26] estimated numerically the laminar heat transfer augmentation of a vertical symmetrical baffled heated channel. This analysis displayed that this baffled channel results in heat transfer augmentation about 2.8 times as non-dimensional baffle height is 0.25. However, this non-dimensional baffle heightoffers a good compromise between heat transfer enhancement and pumping power.

From the previous bibliographical survey, it is clear that most of works deal with the pure forced regime and the limited works devoted to the mixed convection treat only the steady-state phenomena or use a steady-state algorithm which dumps all fluctuations (see [8, 14, 15]). The existence of baffles, in addition to the buoyancy forces, induces strong interactions and pushes the flow to the transient regime. Moreover, the unsteady behaviour and the interaction between the buoyancy and inertial forces make the simulation a laborious task requiring both hardware resources and time. Thus, this work falls within this sphere and attempts to contribute to understanding the unsteady phenomenon by getting as close as possible to the reality of the problem. The object is to carry out transient simulations of the aiding mixed convection in a vertical channel with baffles attached to the heated wall.

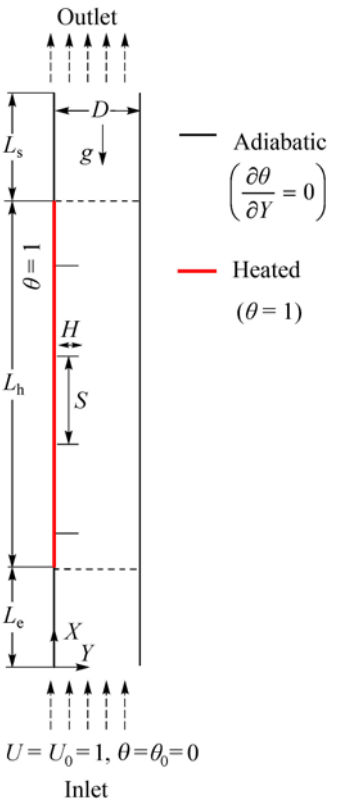


Fig. 1. Flow configuration and boundary conditions.

Problem definition and mathematical formulation

The schematic drawing of the geometry considered in this study is illustrated in Fig. 1. The diagram comprises of two parallel plates channel of length L and width ($D = d/d = 1$). The heated wall is equipped with four equi-spaced ($S = s/d = 1$) identical baffles where the upstream baffle is located at $X = 5$. The dimensionless baffle height is $H = h_b/d$, Corresponding to the blockage ratio for the channel width of unity. However, the smooth wall is preserved adiabatic. The inlet and outlet lengths are carefully chosen to avoid any unrealistic boundary condition at the inlet and the recirculation zone is inside the computational domain [27]. So, the non-dimensional lengths are as follows: the heated section of $L_h = 6D$, situated at $L_e = 4D$ from the inflow position and at $L_s = 12D$ from the outlet. Thus, the total channel length is $L = 22D$. The baffles are assumed to be of negligible thickness and made of a material of high thermal conductivity, so no boundary condition is needed for the temperature.

An upward uniform airflow penetrates in the channel with constant velocity and temperature (U_0, θ_0) from the bottom as indicated in the diagram and leaves from the top channel, so the convection is in the assisted flow regime. The fluid flow (air, Pr = 0.71) is taken to be laminar, incompressible, and viscous (Newtonian).

The thermophysical properties are considered to be constants excluding the fluid density in the buoyancy term, where the Boussinesq law approximation is introduced. Based on the cited assumptions, the governing equations (1) – (4) of continuity, momentum, and energy in the dimensionless form will be reduced to:

Mass:

$$\frac{\partial U}{\partial X}+\frac{\partial U}{\partial X}=0; \tag{1}$$

X-momentum:

$$\frac{\partial U}{\partial \tau}+U\frac{\partial V}{\partial X}+V\frac{\partial U}{\partial Y}=-\frac{\partial P}{\partial X}+\frac{1}{\mathrm{Re}}\left(\frac{\partial^2 U}{\partial X^2}+\frac{\partial^2 U}{\partial Y^2}\right)+\frac{\mathrm{Gr}}{\mathrm{Re}^2}\theta; \tag{2}$$

Y-momentum:

$$\frac{\partial V}{\partial \tau}+U\frac{\partial V}{\partial X}+V\frac{\partial V}{\partial Y}=-\frac{\partial P}{\partial Y}+\frac{1}{\mathrm{Re}}\left(\frac{\partial^2 V}{\partial X^2}+\frac{\partial^2 V}{\partial Y^2}\right); \tag{3}$$

Energy:

$$\frac{\partial \theta}{\partial \tau}+U\frac{\partial \theta}{\partial X}+V\frac{\partial \theta}{\partial Y}=\frac{1}{\mathrm{Pr}\,\mathrm{Re}}\left(\frac{\partial^2 \theta}{\partial X^2}+\frac{\partial^2 \theta}{\partial Y^2}\right). \tag{4}$$

The dimensionless variables used to derive the above equations are

$$X=\frac{x}{d},\ Y=\frac{y}{d},\ U=\frac{u}{u_0},\ V=\frac{v}{u_0},\ \tau=\frac{tu_0}{d},\ \theta=\frac{T-T_0}{T_\mathrm{w}-T_0},\ P=\frac{\left(p+\rho_0 qx\right)}{\rho_0 u_0^2} \tag{5}$$

The dimensionless parameters are as follows

$$\mathrm{Re}=\frac{u_0 d}{\nu},\ \mathrm{Gr}=\frac{q\beta\left(T_\mathrm{w}-T_0\right)d^3}{\nu^2},\ \mathrm{Ri}=\frac{\mathrm{Gr}}{\mathrm{Re}^2},\ \mathrm{Pr}=\frac{\mu}{kc_p}. \tag{6}$$

Physical parameters

The numerical results obtained for the flow and thermal fields are evaluated in the form of dimensionless Nusselt number and friction factor. The heat transfer rate is quantified by local Nusselt number, which represents the ratio of convection to pure conduction heat transfer in the fluid phase; it is defined by the following expression

$$\mathrm{Nu}_X=\frac{hd}{k}=\frac{\dfrac{-k\left.\dfrac{\partial T}{\partial y}\right|_\mathrm{w}}{T_\mathrm{w}-T_0}}{k}=-\left.\frac{\partial T}{\partial y}\right|_\mathrm{w}\frac{d}{T_\mathrm{w}-T_0}=-\left.\frac{\partial\theta}{\partial Y}\right|_\mathrm{w}, \tag{7}$$

h is the heat transfer coefficient and is evaluated from the temperature gradient on the heated wall as

$$h=\frac{-k\left.\dfrac{\partial T}{\partial y}\right|_\mathrm{w}}{T_\mathrm{w}-T_0}. \tag{8}$$

And the mean wall Nusselt number is given by

$$\mathrm{Nu}=\frac{1}{L_\mathrm{h}}\int_0^{L_\mathrm{h}}\mathrm{Nu}_X dX. \tag{9}$$

In unsteady flow, the time-averaged local Nusselt number is calculated by:

$$\overline{\mathrm{Nu}}_X=\frac{1}{\tau_p}\int_0^{\tau_p}\mathrm{Nu}_X d\tau. \tag{10}$$

Finally, the time-averaged mean Nusselt number is given by

$$\overline{\mathrm{Nu}}=\frac{1}{L_\mathrm{h}}\int_0^{L_\mathrm{h}}\overline{\mathrm{Nu}}_X dX. \tag{11}$$

The friction factor is defined as:

$$f=\frac{2\Delta p d}{\rho_0 u_0^2 l_\mathrm{h}}=\frac{2\Delta p}{\rho_0 u_0^2\left(l_\mathrm{h}/d\right)}=\frac{2\Delta p}{\rho_0 u_0^2 L_\mathrm{h}}, \tag{12}$$

with Δp is the pressure loss along the heated section of the length l_h, and L_h is the dimensionless heated part length. The Strouhal number characterizing the flow oscillation is defined as:

$$\mathrm{St} = \frac{f_r d}{u_0}, \tag{13}$$

f_r is the dimensional frequency. In equations (1) – (12), u and v are the velocity components, x and y are the Cartesian coordinates, p is the pressure, ρ is the density, T is the temperature, T_w is the temperature at the wall, d is the channel width, and ρ_0, u_0 and T_0 are theconstant density, velocity and temperature at the inlet conditions, respectively. The subscript "0" refers to the inlet condition and w refers to the heated wall where $Y = 0$ and $L_e < X \le L_h$.

Boundary conditions

The Boundary conditions imposed are as follows:

at the inlet $(X = 0,\ 0 \le Y \le 1)$: $U = U_0 = 1,\ V = 0,\ \theta = 0;$ (14)

at the outlet $(X = L_e + L_h + L_s,\ 0 \le Y \le 1)$: $\dfrac{\partial U}{\partial X} = 0,\ \dfrac{\partial V}{\partial X} = 0,\ \dfrac{\partial P}{\partial X} = 0,\ \dfrac{\partial \theta}{\partial X} = 0,$ (15)

at the adiabatic walls $(0 \le X \le L_e,\ Y = 0$ and $Y = 1)$; $(0 < X - (L_e + L_h) \le L_s,\ Y = 0)$; $(0 \le X \le L_e + L_h + L_s,\ Y = 1)$:

$$U = V = 0,\ \frac{\partial \theta}{\partial X}; \tag{16}$$

at the heated wall $(L_e < X \le L_e + L_h,\ Y = 0)$: $\mathrm{U} = \mathrm{V} = 0,\ \theta = 1.$ (17)

At the baffles surface, the no-slip boundary condition is applied for the all four baffles. This condition is handled using createBaffles utility available under OpenFOAM code which ensures the continuity of the heat flux and imposes a zero velocity on the surface.

Solution method

The partial differential equations (1)–(6) with associated boundary conditions (14)–(17), are solved by the finite volume method using the OpenFOAM®open source code, and the PIMPLE algorithm, which is a mixing of the SIMPLE and PISO algorithms developed by Patankar [28] is employed to link the velocity-pressure fields using the default buoyant-BoussinesqPimpleFoam solver. All the governing equations are discretized with a second order implicit scheme for the time integration. Concerning the spatial discretization, second order schemes are invoked to assess the gradient, divergence, and Laplacian terms.

Model validation

The numerical model has been validated through a comparison with experimental results of Armaly et al. [29] relevant to the isothermal laminar flow in a backward-facing step channel under identical conditions. Further validation is made by comparison of the Nusselt number obtained in mixed convection in a vertical channel with asymmetric heating [30] at the same conditions. As shown in Figs. 2*a* and 2*b*, the comparison indicates the good concordance in both quantity and quality, where the maximum divergence did not exceed 0.5 %.

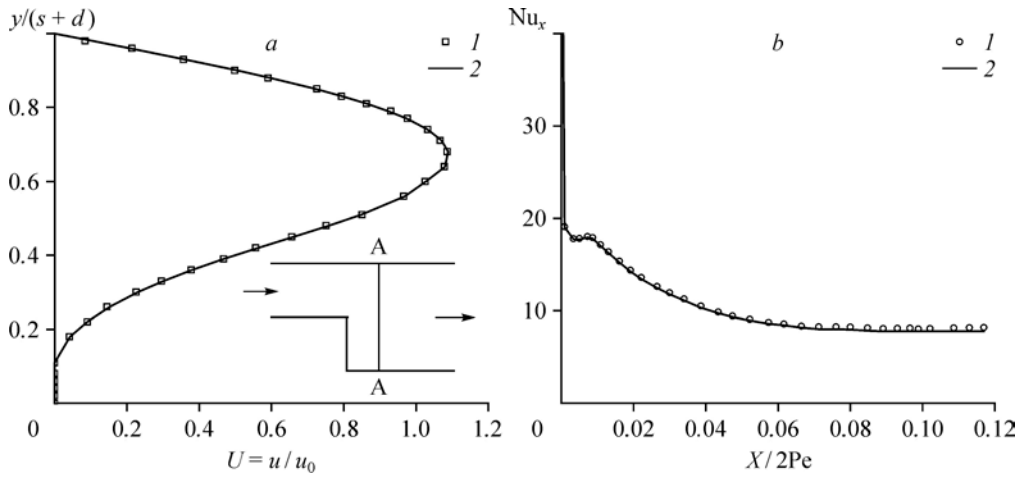


Fig. 2. Comparison of the results obtained with those of literature.
a — streamwise velocity $U = u/u_b$, as function of $y/(s + d)$ at $x/s = 2.55$, where $d = 1.06\,s$ is the inlet channel height; s is the backstep height, u_b is the inlet bulk velocity, $\mathrm{Re} = u_b d/\nu = 50$, as in [29];
b — local Nusselt number (Nu_x) versus $x/(D_h\,\mathrm{Pe}) = X/(2\mathrm{Pe})$ at $\mathrm{Gr} = 1.59\cdot10^5$ and $\mathrm{Re} = u_b d/\nu = 150$, where $D_h = 2d$, as in [30].
1 — data of the present calculations (*a* and *b*), *2* — results of the experiments [29] (*a*) and [30] (*b*).

Grid independence

The grid independence was verified by a series of calculations for different mesh sizes: 330×60, 440×80, 550×100, and 660×120 for $\mathrm{Gr} = 2\cdot10^5$, Re = 1400, and $H = 0.25$. The time-averaged mean Nusselt number obtained for the different mesh sizes is presented in Table 1. As can be seen from Table 1, the relative error between the two last mesh sizes did not surpass 5 %. Thus, the 550×100 grid-size is adopted and employed in calculations for the same geometrical configuration. The grid distribution is dense near the solid walls in order to capture the high gradients of temperature, pressure and velocity. It should be noticed that the expansion ratio between two nearby cells does not surpassed 1.02 to evade unexpected variations in the mesh size for all cases. Mesh distribution over the heated part is shown in Fig. 3. For other channel parts, adequate grid-sizes with the same distribution were used. The baffles are very thin, they are created by converting internal faces into two boundary faces using Create-Baffles tools under OpenFOAM® environment with a specific script file.

Table 1

Effects of grid size on the time-averaged mean Nusselt number at Re = 1400, Gr = 2·10^5, and $H = 0.25$

Mesh sizes	330×60	440×80	550×100	660×120
Mesh number, *i*	1	2	3	4
$\overline{\mathrm{Nu}}$	14.53	14.64	14.70	14.73
Relative errors*, %	—	0.77	0.4	0.22
f	0.05	0.08	0.10	0.12
St	0.1488	0.1458	0.1439	0.1433

* The relative error is defined as $err(\varphi_i, \varphi_{i-1}) = |(\varphi_i - \varphi_{i-1})/\varphi_i|$, where φ = Nu, *f*, St or other calculated value.

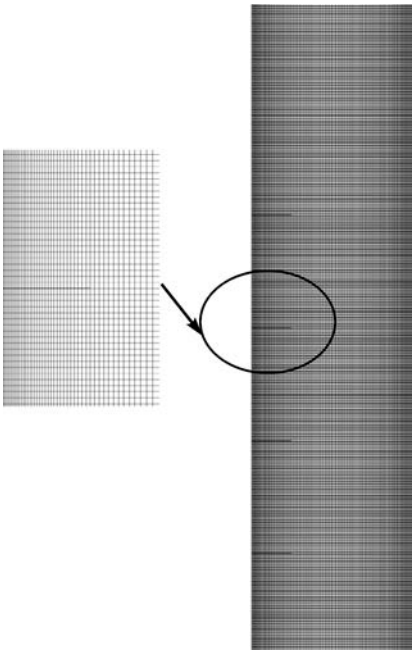


Fig. 3. Heated part mesh for 550×100 grids size.

Results and discussion

General flow and thermal features

Calculations are conducted in unsteady conditions until reaching a steady-state flow or oscillating unsteady flow. The time steps fixed according the Courant–Friedrichs–Lewy condition (CFL) for the highest Reynolds number (at Co < 1) at $\Delta\tau =$ = 0.068. Since a periodic unsteady flow is expected, the CFL condition can be used as a reference to set the time step so that certain fluctuations or transient features are not missed. Simulations were made in laminar flow for Reynolds number in the range of 200 to 1800 and for Grashof number ranging from 10^4 to $2{\cdot}10^5$. For the geometrical configuration, calculations are performed for blockage ratio of H = 0.25 (baseline case), 0.5, and 0.75. All simulations are carried out in HP Z820 workstation with Intel Xeon 2× E5-2620 processor.

Steady-state case

For the case of Re = 500 and Gr = $2{\cdot}10^5$ at H = 0.25, the flow is steady, as demonstrated by the time evolution of u-velocity component at a reference point (X = 9.5, Y = 0.0625) (see Fig. 4). This point is situated downstream of all the baffles in the vicinity of the wall; the flow characteristics in this point are extremely sensitive to all upstream perturbations. Starting from the fluid at rest, the U-velocity component evolved to converge toward a stable value after roughly 150 non-dimensional time units. At low Reynolds/Grashof numbers, the scenario is the same with slight changes in velocity variation and the time needed to reach the steady-state condition. The flow and thermal fields are visualised by streamlines and isotherm contours in the entire channel, a zoom in some regions is used when deemed necessary.

The flow structure for three Reynolds number values (200, 500, and 900) and Gr = $8{\cdot}10^4$ at H = 0.25 is shown in Fig. 5. As can be seen, the steady-state behaviour is evident. The streamlines are parallel in the whole channel, except in the regions situated at the upstream and downstream of the baffles, where a recirculating zone is generated by the pressure variation caused by the sudden variation in section passage.

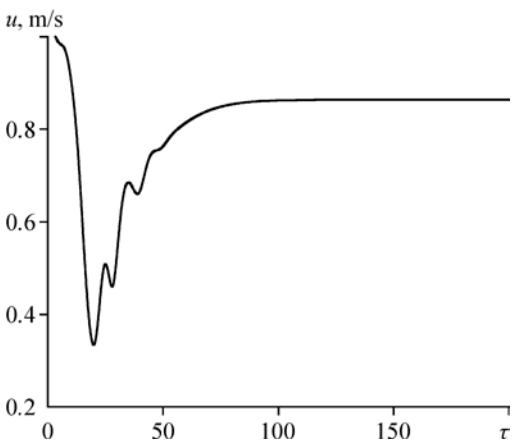


Fig. 4. Time-velocity evolution at (X = 9.5, Y = 0.0625) for Re = 500 and Gr = 2·105.

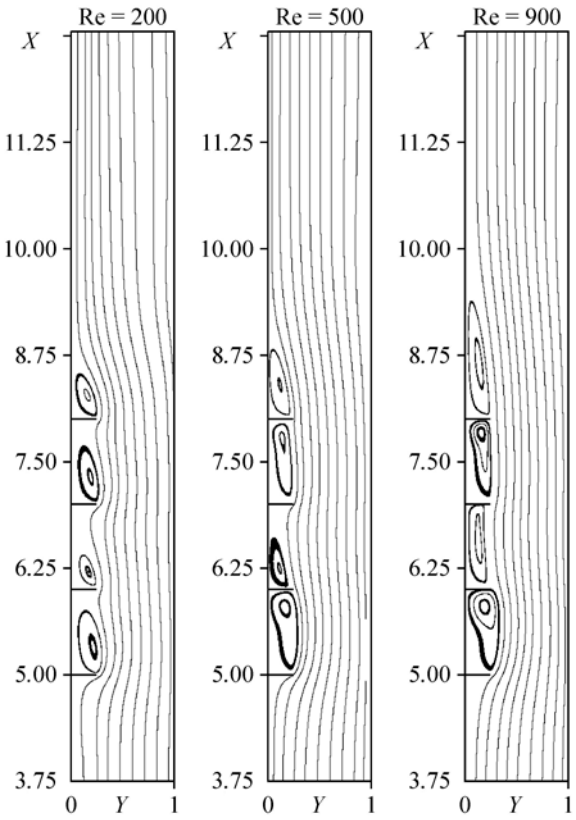


Fig. 5. Streamlines for various Reynolds number.
$Gr = 8 \cdot 10^4$ and $H = 0.25$.

At low Reynolds number (Re = 200), the vortices take an oval form; as the Reynolds number increased, these vortices are trapped by the main flow and become more elongated. The length of these vortices increased alongside increasing Reynolds number in particular for that situated downstream from the final baffle, due to the absence of special constraints. In this range of Re and for a constant Grashof number, the flow is dominated by the buoyant forces and tends to skirt the baffle then penetrate into the cavity regions. With increasing Reynolds number, inertial forces prevail and prevent the main stream flow to penetrate into the cavity. The corresponding isotherm contours are displayed in Fig. 6. These examples show that the insertion of baffles modifies the flow and thermal structures. So, the upstream (first) baffle disturbs the incoming top-hat velocity profile, whereas other baffles interact with the recirculation zones where boundary layers are absent. A very thin boundary layer forms at $x < L_e$; its gradual recovery starts downstream of the recirculation zone past the last baffle.

The vortices formed by the recirculation zones consist of almost the same fluid particles, so they act like stagnation zones shrouding the warm fluid. Due to low velocity in these regions, the heat is transferred mainly by conduction, marked by a low Nusselt number (of the order of unity). Approaching baffles, the isotherms are condensed forming a thin near-wall layer due to the effect of anti clockwise rotation which leads to slow entrainment of cooler fluid into areas in front of the baffles, resulting to an increase in Nusselt number.

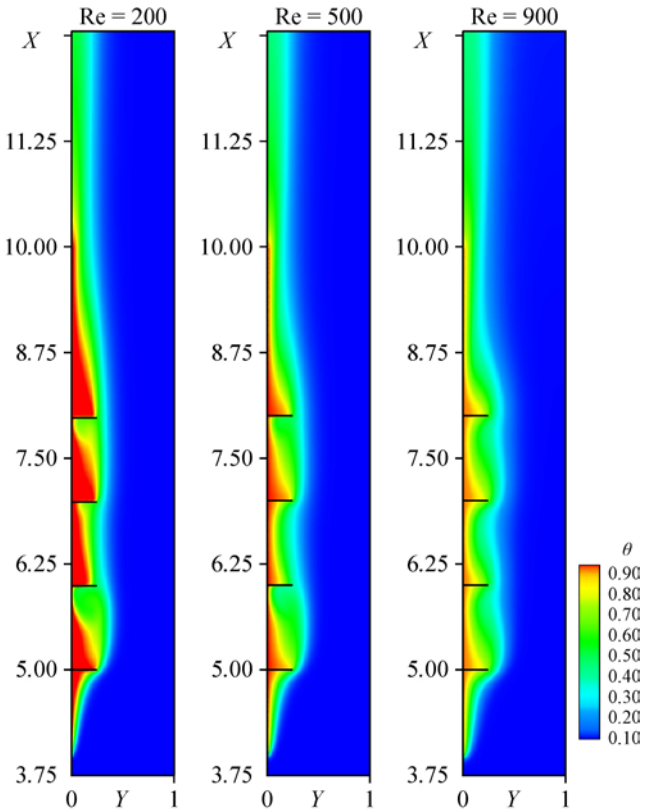


Fig. 6. Isotherms contours for various Reynolds number. Gr = $8 \cdot 10^4$ and $H = 0.25$.

Unsteady-state case

Simulations of the aiding mixed convection in a channel with baffles at high Reynolds number values revealed that the Kelvin – Helmholtz (K–H) instabilities crop up, which forces the flow to go under self-sustained oscillatory behaviour. These instabilities were induced by the successive contraction-expansion in the channel cross section. To highlight the time dependent flow characteristics, the time evolution of the U-velocity component at a reference point ($X = 9.5$, $Y = 0.0625$) for Re = 1400 and Gr = $2 \cdot 10^5$ is plotted in Fig. 7. It should be noted that only the time quasi-periodic phase is shown for the sake of clarity. It can be clearly seen that, the velocity has evolved into an unsteady quasi-periodic flow following laps of time corresponding to the developing time. The developing time depends on Reynolds number, Grashof number, and geometric parameters. For the case of Re = 1400 and Gr =$2 \cdot 10^5$, the developing nondimensional time is about 412 and time period τ_p is about 6.94 throughout the quasi-periodic stage $412 < \tau < 730$.

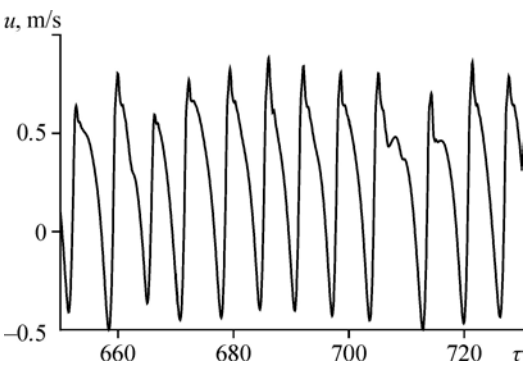


Fig. 7. Time-velocity at ($X = 9.5$, $Y = 0.0625$) for Re =1400, Gr = $2 \cdot 10^5$ and $H = 0.25$.

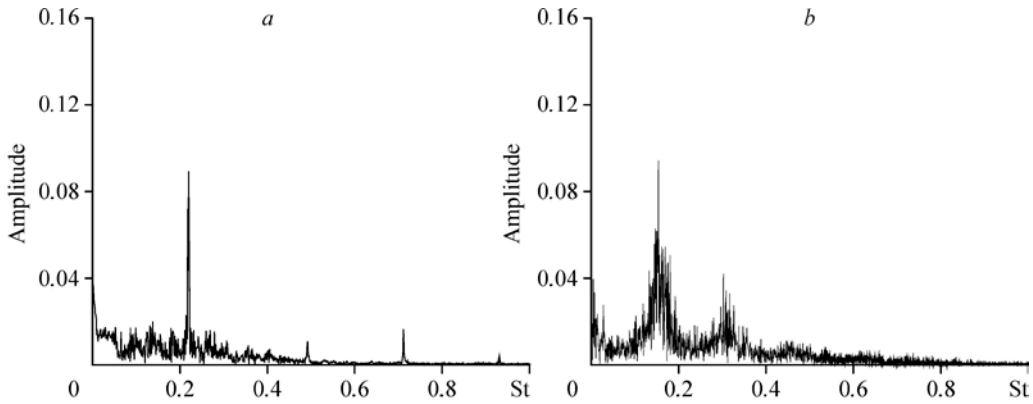


Fig. 8. FFT analysis of the *U*-velocity component history for $H = 0.25$, $\mathrm{Gr} = 5 \cdot 10^4$, and $\mathrm{Re} = 1000$ (*a*), 1400 (*b*).

The FFT analysis of the time history of the *U*-velocity given by Fig. 8, reveals a dominant frequency wave with $\mathrm{St} = 0.2201$ for $\mathrm{Re} = 1000$ and $\mathrm{Gr} = 5 \cdot 10^4$, where St is the Strouhal number. The Strouhal number represents the ratio of inertial forces due to the local acceleration of the flow to the inertial forces due to the convective acceleration; in other words, it refers to the dimensionless frequency with which the vortices are shed (see Fig. 9). The value of St changes with Reynolds number and Grashof number. The same analysis

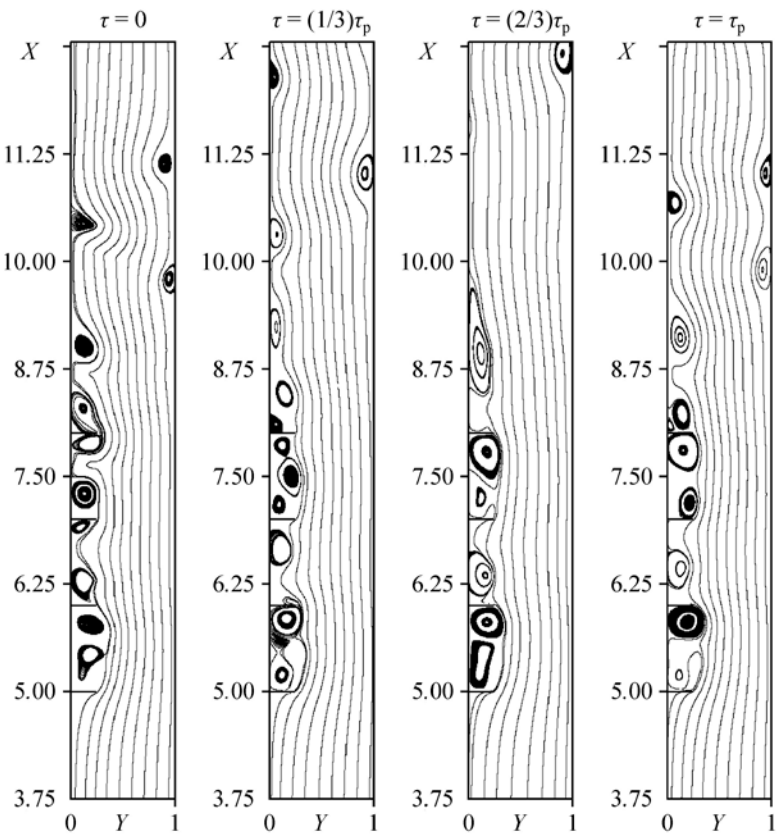


Fig. 9. Streamlines for four steps of oscillation period at $\mathrm{Gr} = 2 \cdot 10^5$ and $\mathrm{Re} = 1400$.

Table 2
Strouhal number for different values of Reynolds and Grashof numbers at $H = 0.25$

Re	Gr	St
1000	$5 \cdot 10^4$	0.2201
1000	$2 \cdot 10^5$	0.1937
1400	$5 \cdot 10^4$	0.1535
1400	$2 \cdot 10^5$	0.1439
1800	$5 \cdot 10^4$	0.1091
1800	$2 \cdot 10^5$	0.1053

demonstrates the superposition of multiple waves induced by instabilities due to inertial forces, buoyancy forces, or interactions between these two forces. Waves were initiated by successive interactions between the main incoming flow and the recirculating one, with a minor contribution of fluid particles entrained from the incoming flow, which attempted to leave the cavity. The amplitude and frequency of the dominant wave decrease alongside an increasing Reynolds number; however, an augmentation in Grashof number leads to increase the amplitude of harmonic waves. As can be seen from Table 2, the Strouhal number is more sensitive to Re than Gr, in the ranges of this study. It decreases from 0.2201 to 0.1535 for $Gr = 5 \cdot 10^4$ when increasing Reynolds number from 1000 to 1400. However, it decreases only from 0.1535 to 0.1439 for Gr varying from $5 \cdot 10^4$ to $2 \cdot 10^5$ at Re = 1400. This sensitivity becomes negligible at high Reynolds number. In a study by Perng and Wu [31] relative the mixed convection over heated blocks with rectangular cylinder as vortex generator they found that St = 0.1488 under pure forced convection flow (Re = 500, Gr = 0) and it decreases to 0.1443 for $Gr = 2 \cdot 10^5$. The critical Reynolds number relative for the transition to self-sustained oscillatory flow and the Strouhal number is no direct relation to the Richardson number. It should be noted that, the different illustrations demonstrate that the flow remains laminar for all Reynolds/Grashof numbers combinations studied in this paper.

The travelling waves sweep the solid face along the surrounding baffled wall, causing the roll evolution, with continuous fragmentation of the near-wall region. To demonstrate the wavy flow character, four sequences of the streamlines covering one cycle are illustrated in Fig. 9. As mentioned for the dominant frequencies, vortices are shed sequentially in a periodic manner, from the tip of the baffles, and unleashed into the core flow. The inertial forces generated by the increase in fluid velocity lead to an increase in the size of the recirculation area. This increase in size makes it unstable and prepares it to split into two zones. The detached zone propagates backwards giving rise to a progressive wave in the vicinity of the hot wall. A zone of smaller size is created in the vicinity of the adiabatic wall alternating with the zone next to the hot wall. The origin of these vortices occurred as compensation for the local acceleration of the flow at the side of the hot wall to satisfy the continuity equation. Similar vortices cells have been observed by other authors in mixed convection in channel containing heated blocks using a rectangular bar as vortex generator at high Reynolds number (see [32]) and in forced convection in channel equipped with oblique plates at moderate Reynolds number values (see [9, 10, 31]).

The flow repeated every quasi-constant interval time τ_p, the time period $\tau_p = 1/St$ varies from 4.5 to 9.5 with Re from 1000 to 1800. It is $\tau_p \approx 7$ only for Re = 1400 and $Gr = 2 \cdot 10^5$ and representing the dominant wave mode. The corresponding thermal field for the four times is given in Fig. 10. As can be clearly seen, the isotherm contours emulated the flow evolution. Leaving the cavities, vortices wrapped up the warm fluid to eject it into the core flow. As mentioned above, the interruption of the dynamic fragmentation of the recirculation zone disrupted the development of the thermal shear layer near the hot wall. The combination of two mechanisms efficiently contributed to fluid mixing, attenuating the temperature in the vicinity of the heated wall.

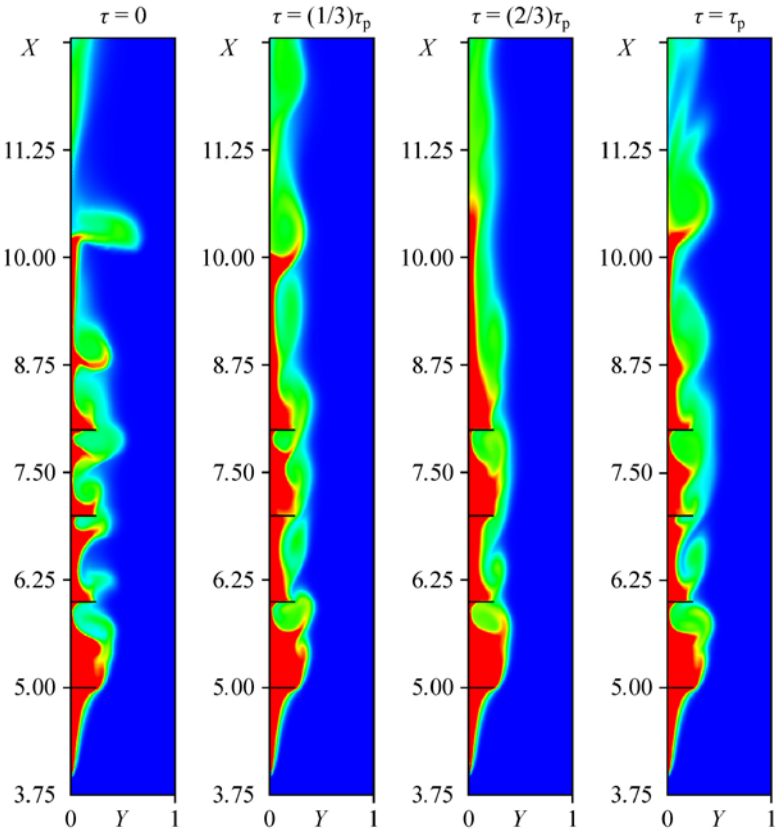


Fig. 10. Isotherms contours for four steps of oscillation period at Gr = $2 \cdot 10^5$ and Re =1400.

Parametric study

Effect of Reynolds number

The quantification of the heat transfer rate is achieved by calculation of the local Nusselt number along the heated surface for different Reynolds and Grashof numbers. Additionally, the time-averaged mean Nusselt number versus Reynolds/Grashof number for each configuration is evaluated.

The time-averaged local Nusselt number evolution along the heated part length at Gr = $= 2 \cdot 10^5$ and Re = 500 and 1800 is presented in Fig. 11*a*. In these plots, the instantaneous values are evaluated after reaching the steady state for Re = 500 and the periodic flow for Re = 1800. Along the inlet region, the time-averaged local Nusselt number evolution is the same, with a somewhat slight increase observed for Re = 1800. However, away from the inlet, a considerable increase is obtained by the activation of oscillatory flow. In the unsteady regime, the time-averaged local Nusselt number reaches its maximum just at rear the baffle for the first one, this point moves just upstream of the baffle for the others. An exception is made for the first chicane in steady state where the time-averaged local Nusselt number continues to fall even before the chicane. On the other hand, the local minimum is recorded near the baffle base. These two points corresponded to the thinner and thicker thermal shear layer, respectively. The Grashof number effect is noticeable only at low Reynolds number values; i.e. at a high Richardson number ($Ri = Gr/Re^2$), downstream from the last baffle where buoyancy becomes

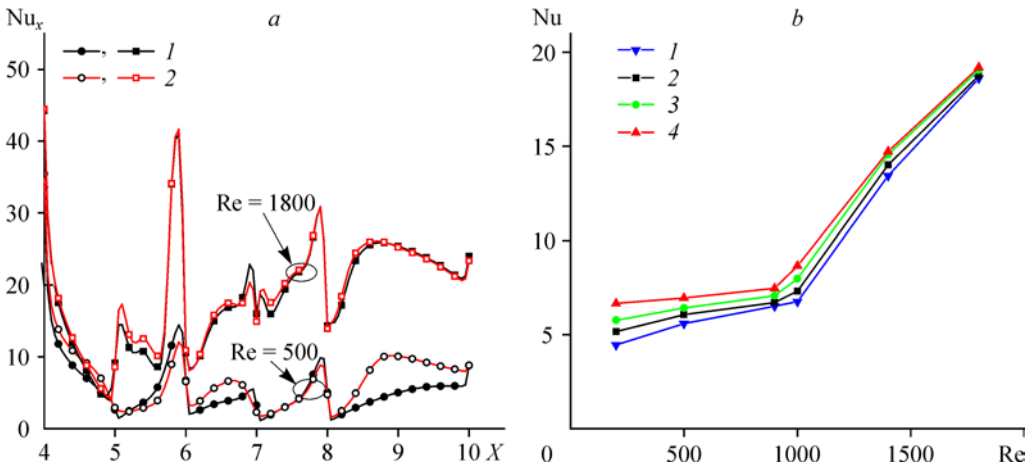


Fig. 11. Time-averaged local and mean Nusselt number under different conditions.
a — time-averaged local Nusselt number, *b* — time-averaged mean Nusselt number;
a — Gr = 10^4 (*1*), $2\cdot10^5$ (*2*), *b* — Gr = 10^4 (*1*), $5\cdot10^4$ (*2*), 10^5 (*3*), $2\cdot10^5$ (*4*).

more important alongside an increasing temperature in the near-wall region. At this high Ri level, the adverse pressure caused by the buoyant flow effect takes a weighty level compared to the inertial forces leading to an augmentation in local velocity. This phenomenon becomes more pronounced as the heat builds up downstream of the last chicane. The time-averaged mean Nusselt number as a function of Reynolds number for different Grashof number values is depicted in Fig. 11*b*. At a steady-state flow, the Nusselt number increases slowly alongside an increasing Reynolds number; following transition to the unsteady flow regime, the elevation in Reynolds number leads to a substantial augmentation of the time-averaged Nusselt number. As explained above, this augmentation is the result of fluid mixing and regeneration, effected via the activation of oscillatory flow. Nevertheless, this is not the case for the Grashof number; indeed, the effect of the Grashof number is more pronounced only in the steady-state flow. In general, the amelioration in heat transfer is concerned with the penalty from the friction coefficient, which induces an increase in pressure drop. The friction coefficient for the baffled channel versus Reynolds number for different Grashof number values is plotted in Fig. 12 for H = 0.25. At low velocity, the friction forces are important; however, as inertial forces increase, the friction factor decreases considerably. For the effect of heating, it is found that the buoyancy forces enhance pressure loss.

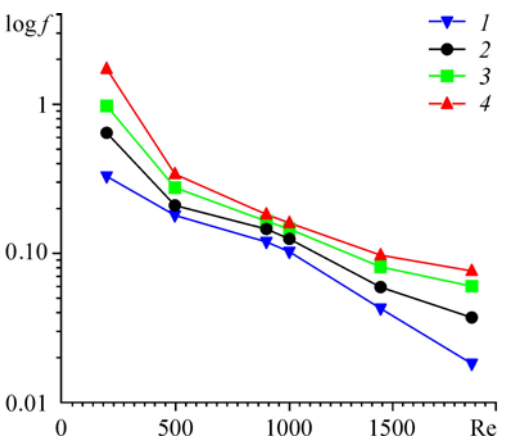


Fig. 12. Friction factor as function of Reynolds number for H = 0.25.
Gr = 10^4 (*1*), $5\cdot10^4$ (*2*), 10^5 (*3*), $2\cdot10^5$ (*4*).

Effect of baffle height

The effect of baffle height on heat transfer is achieved by calculation for three baffle heights H = 0.25, 0.5, and 0.75 and different Reynolds number values; the results

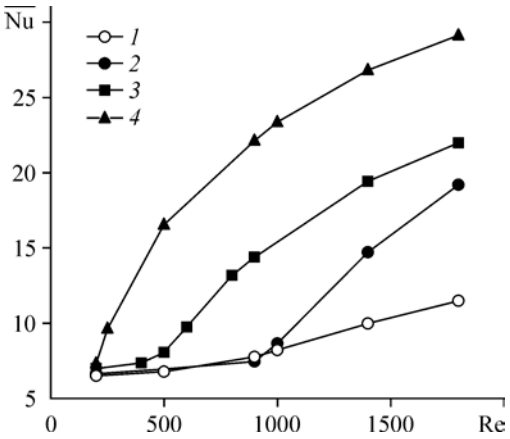


Fig. 13. Variation of time-averaged mean Nusselt number vs. Reynolds number for $Gr = 2 \cdot 10^5$ and various H. $H = 0$ (*1*), 0.25 (*2*), 0.5 (*3*), 0.75 (*4*).

are summarised in Fig. 13. The augmentation of the baffle height has two-fold impacts: it extends the heat exchange area, because the baffles are made of materials of high conductivity, and reduces the critical Reynolds number related to the transition to unsteady flow. As can be concluded from the time-averaged mean Nusselt number curve, for $H = 0.25$, the transition to unsteady flow occurred at a Reynolds number between 900 and 1000. This interval is reduced to between 400 and 500 for $H = 0.5$ and below 300 for $H = 0.75$. The transition to unsteady flow leads to a significant augmentation of the time-averaged mean Nusselt number. To quantify the heat transfer augmentation, Table 3 recapitulates the time-averaged mean Nusselt number values obtained for the three different baffle heights (0.25, 0.5, and 0.75), and different Reynolds number values for the highest value of Grashof number ($Gr = 2 \cdot 10^5$). Moreover, the Nusselt number augmentation when passing from one baffle height to other is evaluated. It can be concluded from these results that at a constant baffle height, an increase in Reynolds number always leads to an increase in time-averaged mean Nusselt number and that the heat transfer intensification rate is below 12 % if the flow still is in the same regime. However, this rate can exceed 100 % if the flow regime translates from the steady to the unsteady regime. Similar results can be obtained when switching from one baffle height to another. The effect of the heat exchange area, A, is not visible in the time-averaged mean Nusselt number evolution; indeed, it is remarkable in the heat transfer rate calculation ($= hA\Delta T$). The rate of heat transfer is linearly dependent on the heat exchange area. Unfortunately, as expected, the augmentation of heat transfer is always accompanied by more friction in the interface fluid/solid surface, on the one hand, and within the fluid as results of particles interaction themselves, on the other hand. This interaction is resulting in growth of pressure drop with H (see Fig. 14).

Table 3

Time-averaged mean Nusselt number as function of baffle height and Reynolds number at $Gr = 2 \cdot 10^5$

Re	$Nu_{H=0.25}$	$Nu_{H=0.5}$	$Nu_{H=0.75}$	ΔNu_1^*, %	ΔNu_2^*, %
200	6.65	6.99	7.33	5	5
500	6.94	8.06	16.54	16	105
900	7.46	14.38	22.13	93	53
1000	8.65	14.74	23.37	70	58
1400	14.72	19.42	26.82	32	38
1800	19.20	22.00	29.12	15	32

* ΔNu_1 and ΔNu_2 — increase in heat transfer compared to the basic channel configuration with the baffle height of $H = 0.25$ and with increased heights of $H = 0.75$ and $H = 0.5$, respectively.

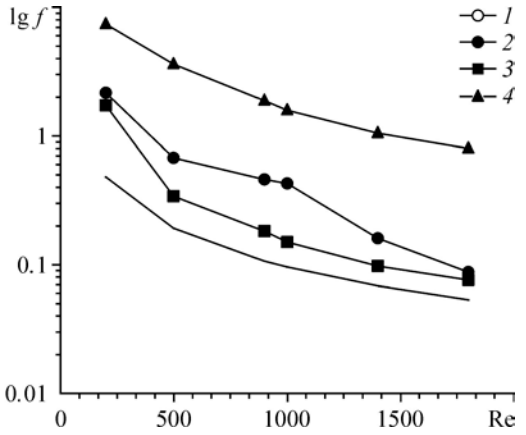


Fig. 14. Variation of the friction factor vs. Reynolds number for Gr = $2 \cdot 10^5$ and various *H*.
H = 0 (*1*), 0.25 (*2*), 0.5 (*3*), 0.75 (*4*).

Conclusions

Heat transfer and fluid flow under mixed convection conditions in a channel with baffles were investigated by numerical simulations of the flow and thermal fields. The calculation was validated by comparison with results from the literature, and good agreements were achieved. The effect of various thermal and dynamic parameters studied, such as Reynolds number, Grashof number, and a geometric parameter, i.e. the baffle height. The results demonstrated that the baffles disturbed the near-wall region and contributed to fluid mixing. With the augmentation of Reynolds number to relatively high values, the disruption induces the transition of the flow to the self-unsteady state regime. The critical Reynolds number value was dependent on both the Grashof number and the baffle dimension. The amplitude and frequency of the self-sustained wave oscillations were more affected by Reynolds than by Grashof numbers. The time dependent flow leads to an additional heat transfer enhancement.

Nomenclature

$\mathrm{Co} = u_0 \dfrac{\Delta t}{\Delta x}$ — Courant number,

c_p — specific heat at constant pressure, J/(kg K),

d — channel width, m,

$D = d/d = 1$ — dimensionless channel width,

$f = \dfrac{2\Delta p d}{\rho_0 u_0^2 l_\mathrm{h}} = \dfrac{2\Delta p}{\rho_0 u_0^2 L_\mathrm{h}}$ — friction factor,

f_r — dimensional frequency, Hz,

g — gravitational acceleration, m /s^2,

$\mathrm{Gr} = \dfrac{g\beta(T_\mathrm{w} - T_0)d^3}{\nu^2}$ — Grashof number,

h — heat transfer coefficient, W/(m^2·K),

$H = h_\mathrm{b}/d$ — dimensionless baffle height or blockage ratio,

h_b — baffle height, m,

k — thermal conductivity, W/(m·K),

$L_\mathrm{h} = l_\mathrm{h}/d$ — dimensionless heated part length,

$L_\mathrm{e} = l_\mathrm{e}/d$ — dimensionless inlet length,

$L_\mathrm{s} = l_\mathrm{s}/d$ — dimensionless outlet length,

Nu_x — Nusselt number,

$\overline{\mathrm{Nu}}$ — time-averaged mean Nusselt number,

p — pressure, Pa,

$P = (p + \rho_0 g x)/\rho_0 u_0^2$ — dimensionless pressure,

$\mathrm{Pe} = \mathrm{Re} \cdot \mathrm{Pr}$ — Peclet number,

$\mathrm{Pr} = \nu/\alpha$ — Prandtl number,

$\mathrm{Re} = u_0 d/\nu$ — Reynolds number,

$\mathrm{Ri} = \mathrm{Gr}/\mathrm{Re}^2$ — Richardson number,

s — baffle distance, m,

$S = (s/d) = 1$ — dimensionless baffle distance,

$\mathrm{St} = f_\mathrm{r} d/u_0$ — Strouhal number,

T — temperature, K,

t — time, s,

u, v — velocity components in x- and y-directions, m/s,

U, V — dimensionless velocity components,

x, y — dimensional Cartesian coordinates, m,

X, Y — dimensionless Cartesian coordinates.

Greek letter

α — thermal diffusivity, m^2/s,

β — thermal expansion coefficient, 1/K,

Δp — pressure drop, Pa,

$\Delta\tau$ — time step,

$\theta = \dfrac{(T - T_0)}{(T_\mathrm{w} - T_0)}$ — dimensionless temperature,

μ — dynamic viscosity, kg /(m·s),

ν — kinematic viscosity, m^2/s,

ρ — density, kg/m^3,

$\tau = t \cdot u_0 / d$ — dimensionless time,

τ_p — time of a period.

Subscripts

0 — at inlet conditions, p — refers to one period, w — wall.

References

1. **A. Valencia,** Unsteady flow and heat transfer in a channel with a built-in tandem of rectangular cylinders, Numer. Heat Transf. A, 1996. Vol. 29, No. 6, P. 613 – 623.
2. **Y. Ishino, M. Suzuki, T. Abe, and S. Yamaguchi,** Flow and heat transfer characteristics in pulsating pipe flows (effects of pulsation on internal heat transfer in a circular pipe flow), Heat Transfer–Japanese Research, 1996, Vol. 25, No. 5, P. 323 –341.
3. **G. Wang, K. Stone, and S.P. Vanka,** Unsteady heat transfer in baffled channels, J. Heat transfer, 1996, Vol. 118, No. 3, P. 585 –591.
4. **M. Yilmaz,** The effect of inlet flow baffles on heat transfer, Inter. Comm. Heat and Mass Transf., 2003, Vol. 30, No. 8, P. 1169 –1178.
5. **S.V. Patankar, C.H. Liu, and E.M. Sparrow,** Fully developed flow and heat transfer in ducts having streamwise-periodic variations of cross-sectional area, J. Heat Transf., 1977, Vol. 99, No. 2, P.180 –186.
6. **B.W. Webb and S. Ramadhyani,** Conjugate heat transfer in a channel with staggered ribs, Inter. J. Heat Mass Transf., 1985, Vol. 28, No. 9, P. 1679 –1687.
7. **C. Berner, F. Durst, and D.M. Mc Eligot,** Numerical study of fluid flow and heat transfer in a parallel plate channel with baffles, J. Heat Transfer, 1984, Vol. 106, No. 4, P. 743 –749.
8. **C.H. Cheng, C.D. Luy, and W.H. Huang,** Buoyancy effect on the heat convection in vertical channels with fin array at low Reynolds numbers, Inter. J. Heat Mass Transf., 1992, Vol. 35, No. 10, P. 2643 –2653.
9. **C.H. Cheng and J.J. Yang,** Buoyancy-induced recirculation bubbles and heat convection of developing flow in vertical channels with fin arrays, Inter. J. Heat Fluid Flow, 1994, Vol. 15, No. 1, P. 11–19, 1994.
10. **H.C. Fung and A. Lazaridis,** Mixed convection of laminar, fully-developed flow in a finned channel, Transactions on Engineering Sciences, WIT Transactions on Engineering Sciences, 1994, Vol. 12, P. 1–7.
11. **T.S. Chang and Y.H. Shiau,** Flow pulsation and baffle's effects on the opposing mixed convection in a vertical channel, Inter. J. Heat Mass Transf., 2005, Vol. 48, No. 20, P. 4190 – 4204.
12. **C.H. Cheng and W.H. Huang,** Numerical prediction for laminar forced convection in parallel-plate channels with transverse fin arrays, Inter. J. Heat Mass Transf., 1991. Vol. 34, No. 11, P. 2739 –2749.
13. **Y.L. Tsay, T.S. Chang, and J.C. Cheng,** Heat transfer enhancement of backward facing step flow in a channel by using baffle installation on the channel wall, Acta Mech. 2005. Vol.174, No. 1–2, P. 63 –76.
14. **S.S. Mousavi and K. Hooman,** Heat and fluid flow in entrance region of a channel with staggered baffles, Energy Convers. Manag, 2006, Vol. 47, No. 15-16, P. 2011–2019.
15. **N.B. Santos and M.J.S. Lemos,** Flow and heat transfer in a parallel-plate channel with porous and solid baffles, Numer. Heat Transf. A, 2006, Vol. 49, No. 5, P. 471 – 494.
16. **H.J. Zhang, Z.P. Zou, F. Shao, and S.H. Song,** Investigations of heat transfer enhancement in a channel with staggered porous ribs by the preconditioned density-based algorithm, Numer. Heat Transf. A, 2015, Vol. 67, No. 12, P. 1370 –1385.
17. **K.H. Ko and N.K. Anand,** Use of porous baffles to enhance heat transfer in a rectangular channel, Inter. J. Heat Mass Transf., 2003, Vol. 46, No. 22, P. 4191 – 4199.
18. **J.R. Lopez, N.K. Anand, and L.S. Flecher,** A numerical analysis of laminar convective heat transfer in a three-dimensional channel with baffles, Proc. Of 3d U.S. National Congress on Computational Mechanics, Dallas, TX, 1995. P. 406 – 416.
19. **J.R. Lopez, N.K. Anand, and L.S. Flecher,** Heat transfer in a three-dimensional channel with baffles, Numer. Heat Transf. A, 1996. Vol. 30, No. 2, P. 89 –205.
20. **Z. Guo, and N.K. Anand,** Three dimensional heat transfer in a channel with a baffle in the entrance region, Numer. Heat Transf. A, 1997. Vol. 31, No. 1, P.21–30.
21. **F. Bazdidi-Tehrani, and M. Naderi-Abadi,** Numerical analysis of laminar heat transfer in entrance region of a horizontal channel with transverse fins, Inter. Comm, Heat Mass Transf., 2004. Vol. 31, No. 2, P. 211– 220.
22. **M. Molki and A.R. Mostoufizadeh,** Turbulent heat transfers in rectangular ducts with repeated-baffle blockages, Inter. J. Heat Mass Transf., 1989, Vol. 32, No. 8, P. 1491–1499.
23. **M.A. Habib, A.M. Mobarak, A.M. Atiya, and A.Z. Aly,** Enhanced heat transfer in channels with staggered fins of different spacings, Inter. J. Heat Fluid Flow, 1993. Vol. 14, No. 2, P. 185 –190.
24. **Z.X. Yuna, W.Q. Tao, and Q. Wang,** Experimental investigation of heat transfer enhancement in ducts with winglet fins, First International Conference of Engineering Thermophysics, Beijing, China, 1999, P. 457– 463.
25. **V.I. Terekhov, A.L. Ekaid, and K.F. Yassin,** Heat transfer at a laminar free convection and separated flow past a rib in a vertical channel with isothermal walls, Thermophysics and Aeromechanics, 2017, Vol. 24, No. 4, P. 577–581.
26. **R. Henniche and A. Korichi,** Heat transfer enhancement in self-sustained oscillatory flow in a staggered baffled vertical channel under the buoyancy effect, Numer. Heat Transf. A, 2017, Vol. 71, No. 12, P. 1189 –1204.

27. A. Korichi and L. Oufer, Numerical heat transfer in a rectangular channel with mounted obstacles on upper and lower walls, Inter. J. Therm. Sci., 2005, Vol. 44, No. 7, P. 644–655.

28. S.V. Patankar, Numerical heat transfer and fluid flow, New York: Hemisphere Publishing Corporation, 1980.

29. B.F. Armaly, F. Durst, J.C.F. Pereira, and B. Schonung, Experimental and theoretical investigation of backward-facing step flow, J. Fluid Mech., 1983, Vol. 127, P. 473–496.

30. G. Desrayaud and G. Lauriat, Flow reversal of laminar mixed convection in the entry region of symmetrically heated, vertical plate channels, Inter. J. Therm. Sci., 2009, Vol. 48, No. 11, P. 2036–2045.

31. S.W. Perng and H.-W. Wu, Numerical investigation of mixed convective heat transfer for unsteady turbulent flow over heated blocks in a horizontal channel, Inter. J. Therm. Sci., 2008. Vol. 47, No. 5, P. 620–632.

32. T.S. Park, Plate-spacing effect on unsteady flows and heat transfer characteristics in a channel with inclined plates, J. Mech. Sci. Technol., 2017, Vol. 31, No. 10, P. 4825–4832.